Exploring the Potentialities of Landsat 8 and Sentinel-2 Satellite Data for Estimating the Land Surface Albedo in Urban Areas Using GEE Platform

Carlo Barletta, Alessandra Capolupo(✉), and Eufemia Tarantino

Department of Civil, Environmental, Land, Building Engineering and Chemistry (DICATECh), Politecnico di Bari, via Orabona 4, 70125 Bari, Italy
{carlo.barletta,alessandra.capolupo,eufemia.tarantino}@poliba.it

Abstract. Albedo quantifies the capacity of a certain surface to reflect incident solar radiation. Therefore, this parameter is relevant in environmental and climate studies as it drives both the land surface energy balance and the interaction between surfaces and atmosphere. It can be estimated and monitored at different scales using Remote Sensing technique. However, its assessment is pretty difficult as factors, such as resultant map accuracy, processing time, and complexity of the algorithm used to retrieve it, should be considered.

The goal of this paper is to develop a proper JavaScript code in Google Earth Engine cloud environment in order to estimate surface albedo using two different satellite data, Landsat 8 and Sentinel-2, over two different study areas: Bari (Southern Italy), and Berlin (Northeastern Germany). To achieve this purpose, Landsat 8 and Sentinel-2 images, acquired in close date, were processed in GEE environment by implementing an appropriate JavaScript code. After obtaining albedo maps over both investigated sites, the two algorithms' performances, the Silva for Landsat 8 data and the Bonafoni for Sentinel-2 images, were statistically analyzed and compared. Furthermore, to investigate the outcomes deeply, statistics metrics were computed for different land cover classes also. UrbanAtlas provided by Copernicus was used to classify the whole case studies. Both approaches showed satisfying results albeit Landsat 8 algorithm provided higher mean values than the other one.

Keywords: GEE · Geospatial big data · Climate change · Cloud computing · Copernicus program · UrbanAtlas

1 Introduction

Albedo, a bio-geophysical variable that quantifies the capacity of a surface to reflect solar radiation, plays a fundamental role in environmental studies and climate change investigations as it drives the land surface energy balance and the interaction between surfaces and the atmosphere [1, 2]. Therefore, the Global Climate Observing System (GCOS) considers Albedo as an Essential Climate Variable (ECV) [3].

© The Author(s), under exclusive license to Springer Nature Switzerland AG 2022
O. Gervasi et al. (Eds.): ICCSA 2022 Workshops, LNCS 13379, pp. 435–449, 2022.
https://doi.org/10.1007/978-3-031-10545-6_30

The urbanization process, resulting in land use/land cover (LU/LC) changes and, consequently, the energy balance modification, triggers the Urban Heat Island (UHI) phenomenon [2, 4–8]. Anthropogenic surfaces, in fact, are mainly composed of non-reflective materials and, thus, absorbed incident solar radiation is released as heat [5]. Furthermore, in built-up areas, effective surface albedo values are influenced not only by the presence of land cover features such as buildings, roads and vegetation (including both parks and urban forests) but also by the topography of the so-called "urban canopy" [9].

Albedo can be estimated and monitored both at regional and global scales using Remote Sensing (RS) technique effectively. Indeed, RS is very suitable for studying environmental phenomena [10–13]. However, the albedo estimation from the Top Of the Atmosphere (TOA) corrected satellite images is not easy and the optimal strategy to evaluate it should be based on the compromise among resulting map accuracy, processing time and complexity of the implemented algorithm [14]. On the other hand, the knowledge of the atmospheric conditions and land surface characteristics, obtained from multispectral satellite data, are required for improving results accuracy [2, 15–19].

Various approaches have been proposed in literature to retrieve the surface albedo from different satellite sensors. Among them, Liang's simplified method (2000) [15] and Silva *et al*. (2016) algorithm [20] are largely applied to process Landsat data, characterized by a geometric resolution of 30 m [2]. Those methods require TOA reflectance knowledge in visible (RGB), near infrared (NIR) and shortwave infrared (SWIR) bands. In particular, the Silva *et al*. algorithm, specific for Landsat 8 data, provides accurate albedo estimations albeit a high implementation and operational time are needed. Conversely, Liang's method permits to produce albedo maps in a faster way but with a lower accuracy, compared to Silva's algorithm [2].

The launch of Sentinel-2A and Sentinel-2B satellites of the European Union (EU) Copernicus Program (https://www.copernicus.eu/) in 2015 and in 2017, respectively, brought relevant changes in the observation of land surface processes. Sentinel-2 sensors have, indeed, higher resolution (10 m) than Landsat (30 m), and, thus, it is more suitable for tackling many environmental applications, like land monitoring [21]. In addition, the Multi Spectral Instrument (MSI) on board Sentinel-2 satellites acquires thirteen bands of the Earth with a temporal resolution of five days at the equator [22].

An easy-to-use narrow-to-broadband algorithm, developed by Bonafoni *et al.* (2020) [23] allows retrieving surface albedo from Sentinel-2 Level-2A surface reflectance in RGB, NIR and SWIR spectral bands, assuming the hypothesis of Lambertian surfaces and clear sky conditions [23].

However, analyzing and processing a large volume of geospatial data require considerable time and using a traditional desktop software is not always a feasible solution [2, 24]. The advent of cloud services as Google Earth Engine (GEE) opens up new opportunities to use and integrate diverse Earth Observation (EO) datasets for mapping and monitoring Earth's surface processes [24]. GEE is a cloud-based platform developed for geospatial analysis, that allows users to process geospatial big data using Google's massive computational capabilities. GEE consists of a multi-petabyte free-to-use and continuously updated data catalog of remote sensing imagery, co-located with a high-performance computation service. This last one is accessible through an Application

Programming Interface (API) with an associated web-based Interactive Development Environment (IDE). JavaScript, Python and REST are the available API in GEE [25].

The aim of this paper is to develop a proper JavaScript code in GEE environment to: i) extract surface albedo information from two different satellite data, Landsat 8 and Sentinel-2, and, ii) evaluate and compare their performances to detect the corresponding pros and cons. To meet this purpose, two territories, Bari (Southern Italy) and Berlin (Northeastern Germany), were selected as pilot sites. Such urban areas are extremely different in terms of climatic and geo-morphological characteristics point of view. This allows testing the two approaches in various environmental contexts. Silva *et al*. algorithm (2016) [20] and Bonafoni *et al*. (2020) [23] narrow-to-broadband conversion method were applied to estimate surface albedo from Landsat 8 and Sentinel-2 images, respectively. The performances of those algorithms were statistically analyzed and compared. Lastly, they were also evaluated in accordance with the LU/LC classification provided by the Copernicus program.

2 Materials and Methods

2.1 Study Areas and Data

Bari (Fig. 1), in Southern Italy, and Berlin (Fig. 2), in Northeastern Germany, cities were picked up as pilot sites because of their great diversity in terms of morphological as well as climatic features.

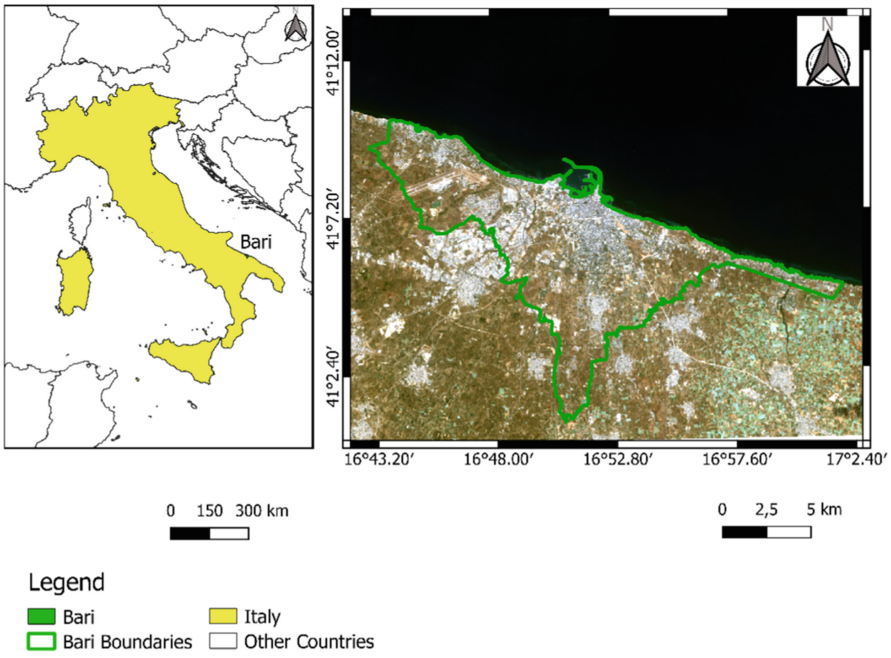

Fig. 1. Study area of Bari.

Bari is a Mediterranean coastal city with hot summers and mild winters [26]. The city has experienced an urban sprawl since the mid twentieth century which causes an expansion of its inner core, built until then, along preferential directions or nuclei. Such an area has a flat topography, and it is mainly characterized by the presence of erosive karstic grooves called "lame". Apart from these grooves, surface water bodies are absent and green urban spaces are scarce [27–29]. Moreover, UHI phenomenon is more evident in the zones close to the city center, even if it is mitigated, especially near the coast, by the sea breeze [26].

Berlin is the capital city of Germany. It has a humid warm temperate climate with cold winters and warm summers. The territory of Berlin, extended for almost 900 km^2, is essentially characterized by a flat topography and a great number of green spaces and water bodies [30, 31]. Its growth started when, in 1871, it was named the capital of Germany. Nevertheless, its sprawl continued during the twentieth century and, in 1920, the "Greater Berlin" became one of the largest and most populated cities in the world [32]. Nowadays, Berlin is characterized by about 35% of built-up areas that results in an evident UHI phenomenon, especially during summer periods [33].

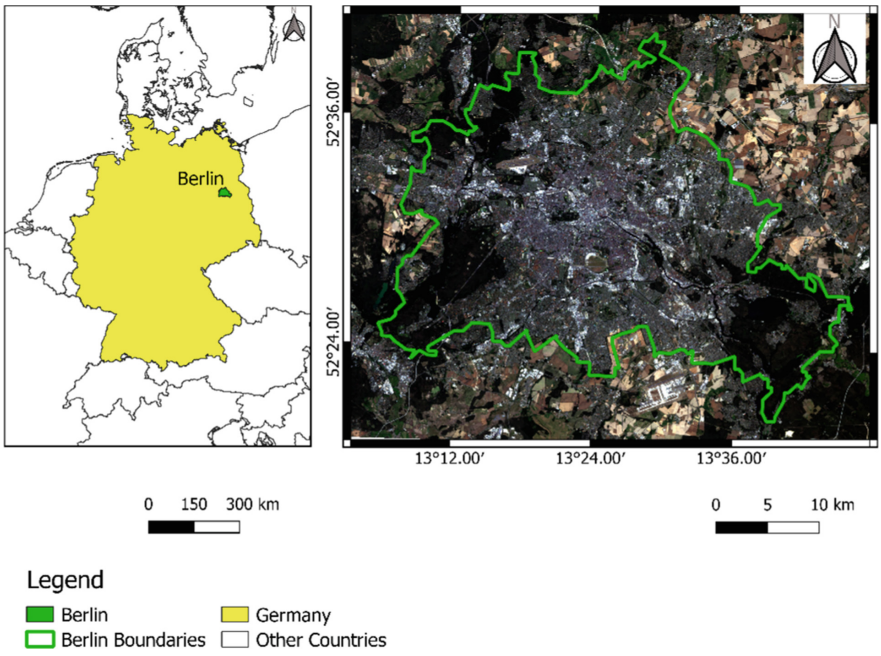

Fig. 2. Study area of Berlin.

Satellite images, collected in the summer period by the two above mentioned missions, were selected for each study area by setting specific criteria, as the acquisition date/time and cloud cover threshold (less than 3%). This last option was fixed to minimize clouds influence on the final thematic maps. More details about the gathered satellite data are reported in Table 1. Concerning the area of Berlin, various Sentinel-2 scenes,

with the same acquisition time but covering different territory portions, were collected and, then, mosaicked by adopting a proper code in GEE.

Table 1. Features of the selected satellite images. OLI: Operational Land Imager; MSI: MultiSpectral Instrument.

Study area	ID	Mission	Sensor	Acquisition date (mm/dd/yyyy)	Acquisition time	Cloud cover (%)
Bari	1	Landsat 8	OLI	07/28/2021	09:34	0.51
Bari	2	Sentinel-2	MSI	07/28/2021	09:40	2.11
Berlin	3	Landsat 8	OLI	07/26/2019	10:02	0.04
Berlin	4	Sentinel-2	MSI	07/26/2019	10:20	0

2.2 GEE Cloud Platform and Workflow

Figure 3 describes the operative workflow applied in this study to estimate surface albedo. Once the collection phase was completed, the new dataset was built and processed in GEE environment by applying Silva *et al.* and Bonafoni *et al.* algorithms on Landsat 8 and Sentinel-2 scenes, respectively. After retrieving surface albedo maps, algorithms performances were statistically evaluated considering both the whole territory of the two case studies, and each LU/LC class. To meet such a purpose the information provided by Copernicus UrbanAtlas 2018 was used [34].

2.3 Surface Albedo Estimation

Two different algorithms were implemented to retrieve surface albedo: the Silva *et al.* method (2016) [20], developed for Landsat 8 satellite images, and the Bonafoni *et al.* algorithm (2020) [23] specific for Sentinel-2 images.

The Silva *et al.* algorithm is expressed as follows:

$$\alpha_{TOA} = p_2 * r_2 + p_3 * r_3 + p_4 * r_4 + p_5 * r_5 + p_6 * r_6 + p_7 * r_7 \quad (1)$$

where α_{TOA} is the TOA albedo, p_i are the weighting coefficients, which represent the ratio between the solar constant of each OLI band and the sum of all solar constant used in the calculation of albedo, and r_i are the TOA reflectances for Landsat 8 spectral bands. The surface albedo α is retrieved by:

$$\alpha = \frac{(\alpha_{TOA} - \alpha_{ATM})}{\tau_{sw}^2} \quad (2)$$

where α_{ATM} is the atmospheric albedo, which value was set equal to 0.03, and τ_{sw} is the atmospheric transmissivity for shortwave radiation, function of local atmospheric pressure, water in the atmosphere, solar zenith angle and air turbidity coefficient [20, 35].

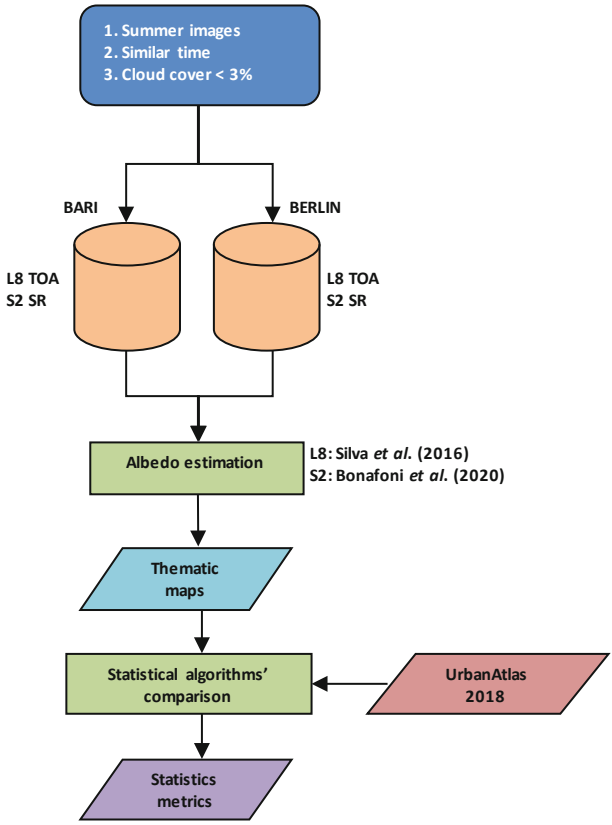

Fig. 3. Operative workflow of satellite data processing. L8: Landsat 8; S2: Sentinel-2.

The easy-to-use Bonafoni *et al*. narrow-to-broadband conversion method is represented by the following equation:

$$\alpha = \omega 2 * \rho 2 + \omega 3 * \rho 3 + \omega 4 * \rho 4 + \omega 8 * \rho 8 + \omega 11 * \rho 11 + \omega 12 * \rho 12 \quad (3)$$

where ω_i are the weighted coefficients, which represent the weight of the portion of the at-surface solar radiation encompassing the range of each MSI spectral band, ρ_i are the surface reflectance for Sentinel-2 bands [23].

A proper JavaScript code was created using GEE platform to retrieve the surface albedo from the selected images with the above-mentioned methods.

2.4 Statistical Comparison of Algorithms' Performances

After obtaining land surface albedo maps from Landsat 8 and Sentinel-2 scenes, a statistical analysis was performed to assess their accuracy and quality. In particular, scatterplots, Mean (μ), Correlation Coefficient (ρ), Standard Deviations (SD) and Root Mean Square Error (RMSE) were calculated.

Moreover, to validate the results, the above-mentioned statistics were extracted for each land cover class, taken from Copernicus Land Monitoring UrbanAtlas 2018, which is a data provided by the Copernicus Program of the European Union, that includes LU/LC categories for many European cities [34].

3 Results and Discussion

Figures 4 and 5 show the land surface albedo maps obtained through the application of the aforementioned algorithms on the selected Landsat 8 and Sentinel-2 satellite images. These maps represent the albedo variability within urban territories of the two investigated sites.

Berlin maps (Fig. 5A and 5B) are darker than those of Bari. This is partly caused by the abundant presence of water bodies in Berlin, which have albedo values close to 0, as well as by other factors such as different LU/LC, climate and latitude. Furthermore, for each study area, the Sentinel-2 map (Fig. 4B for Bari and Fig. 5B for Berlin) result darker than the Landsat 8 map (Fig. 4A for Bari and Fig. 5A for Berlin). Lastly, the albedo map of Bari obtained from Landsat 8 (Fig. 4A) has the highest values.

Figure 6 and Table 2 report the results of the statistical comparison of algorithms' performances, both for Bari and Berlin study areas. In particular, Fig. 6 shows the scatterplots between land surface albedo retrieved by applying the two algorithms, while Table 2 reports the fundamental statistical metrics. The scatterplots show a good correlation among the albedo computed on the same case study with different algorithms. This is evident in Figs. 4 and 5, where it is possible to notice a certain correspondence of albedo trend between Landsat 8 and Sentinel-2 outcomes. Nevertheless, several outliers, in particular in the site of Berlin (Fig. 6B), can be detected due to its greater heterogeneity in LU/LC.

As already highlighted in Fig. 6, a strong correlation between the albedo estimated through the application of the two different algorithms for both sites is outlined in Table 2. Nevertheless, Bari shows the higher ρ, RMSE and μ. These results are also confirmed by the visual inspection of the albedo maps in Figs. 4 and 5 (darker maps for Berlin) and from the boxplots, reported in Fig. 7. This outcome is mainly due to the different climate, that characterizes the two cities, and their diverse latitude. Boxplots highlight outliers in both study areas, probably due to the diverse size and heterogeneity of the investigated territories.

To investigate the results deeply, the main statistical metrics were explored for each LU/LC class. The outcomes of such an analysis are reported in Fig. 8. Figure 9, on the other hand, reports RMSE values, between Landsat 8 and Sentinel-2 albedo products, calculated for each LU/LC class.

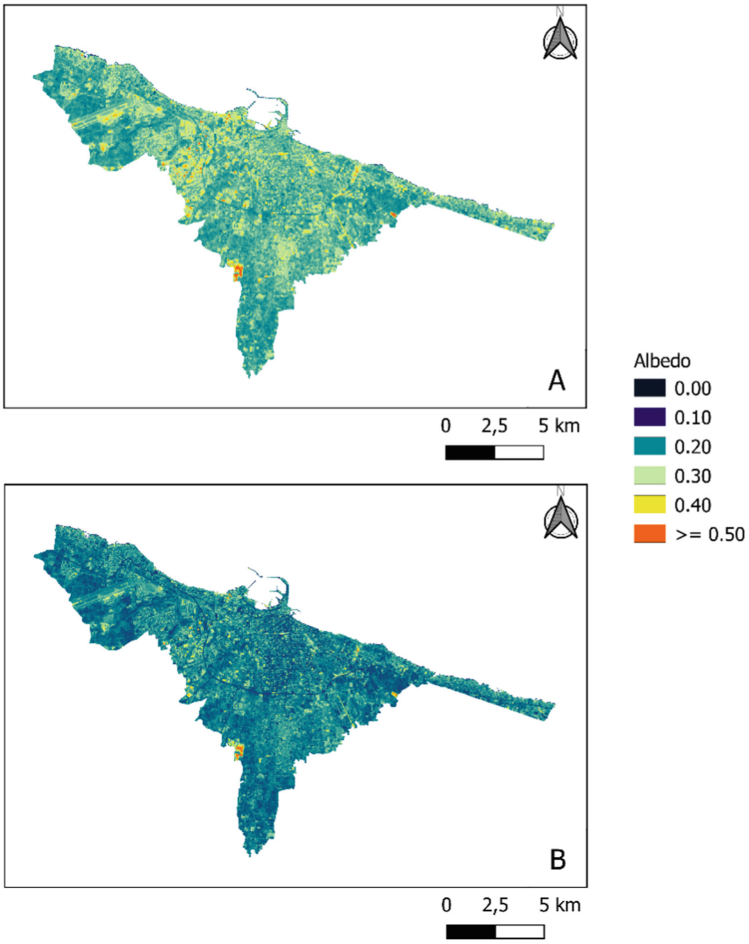

Fig. 4. Land surface albedo maps obtained from L8 Bari (A) and S2 Bari (B) satellite images. L8: Landsat 8; S2: Sentinel-2.

Figure 8 underlines that Silva *et al*. method [20] provides higher albedo values than Bonafoni *et al*. algorithm [23] and that, as expected, Bari has higher values than Berlin for most of the investigated LU/LC classes. Nevertheless, values detected by applying both algorithms are comparable with that one obtained by previous research works. For example, Taha (1997) [36] reported that albedo in urban areas is comprised between 0.10 and 0.20 (0.15 to 0.20 for many US and European cities as 0.20 in Los Angeles and 0.16 in Munich). These values, sometimes, can be exceeded as occurred in the North African cities or Adelaide, in Australia, which values are between 0.30 and 0.45 and equal to 0.27, respectively.

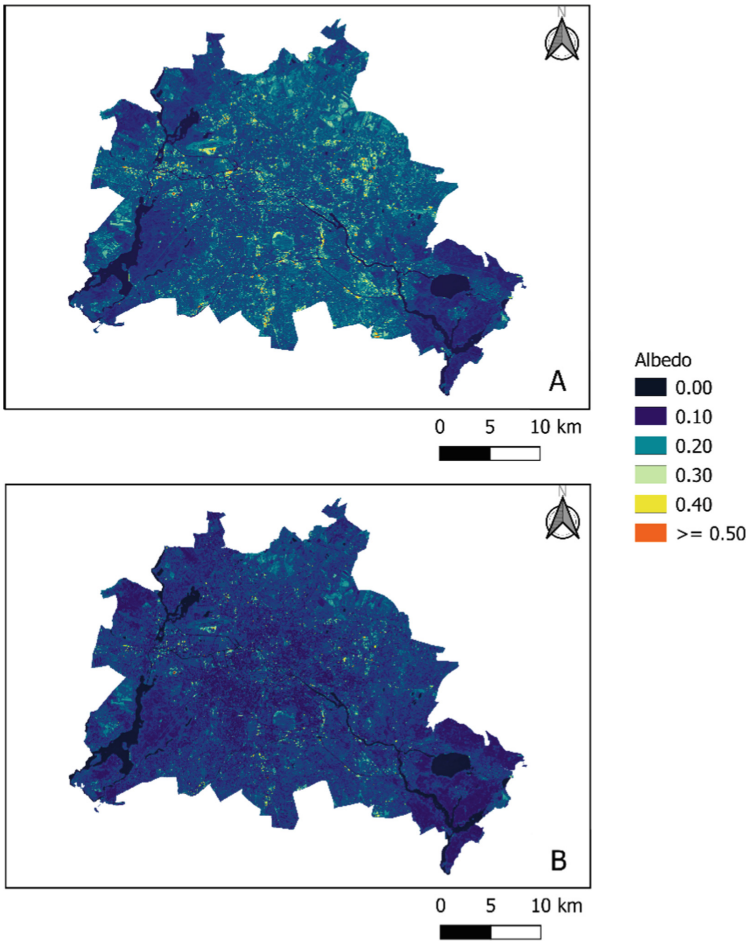

Fig. 5. Land surface albedo maps obtained from L8 Berlin (A) and S2 Berlin (B) satellite images. L8: Landsat 8; S2: Sentinel-2.

Furthermore, Waters *et al.* (2002) [37] reported typical albedo values for various natural or agricultural LU/LC classes. For example, the albedo of coniferous forests is in the range of 0.10–0.15, grass or pastures is between 0.15 and 0.25, agricultural areas, such as corn fields and rice fields, is comprised between 0.14 and 0.22, while the water between 0.025 and 0.348, respectively.

Except for some LU/LC classes, the RMSE trend of L8 and S2 surface albedo is similar for the two study areas (Fig. 9). Just a difference of about 0.02 is, indeed, assessed between Bari and Berlin.

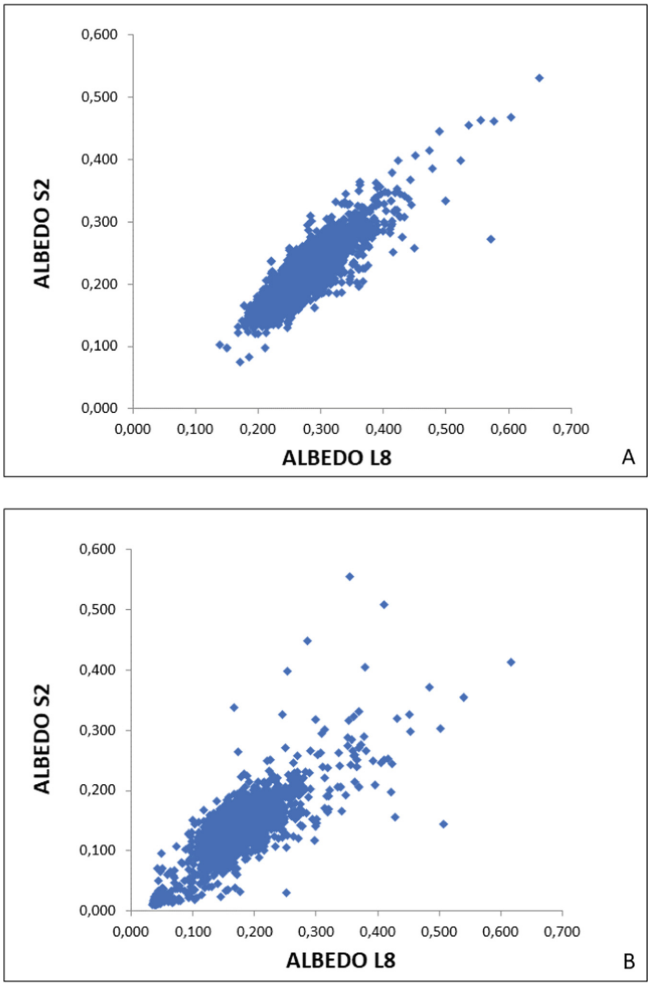

Fig. 6. Scatterplots between the surface albedo retrieved by implementing Silva *et al.* (2016) algorithm for L8 images and Bonafoni *et al.* (2020) method for S2 scenes, for Bari (A) and Berlin (B) study areas, respectively. L8: Landsat 8; S2: Sentinel-2.

Table 2. Main statistics metrics of albedo estimations. L8: Landsat 8; S2: Sentinel-2.

Study area	Images	Mean	SD	ρ	RMSE
Bari	L8	0.256	0.043	0.892	0.057
	S2	0.202	0.037		
Berlin	L8	0.155	0.045	0.805	0.039
	S2	0.127	0.039		

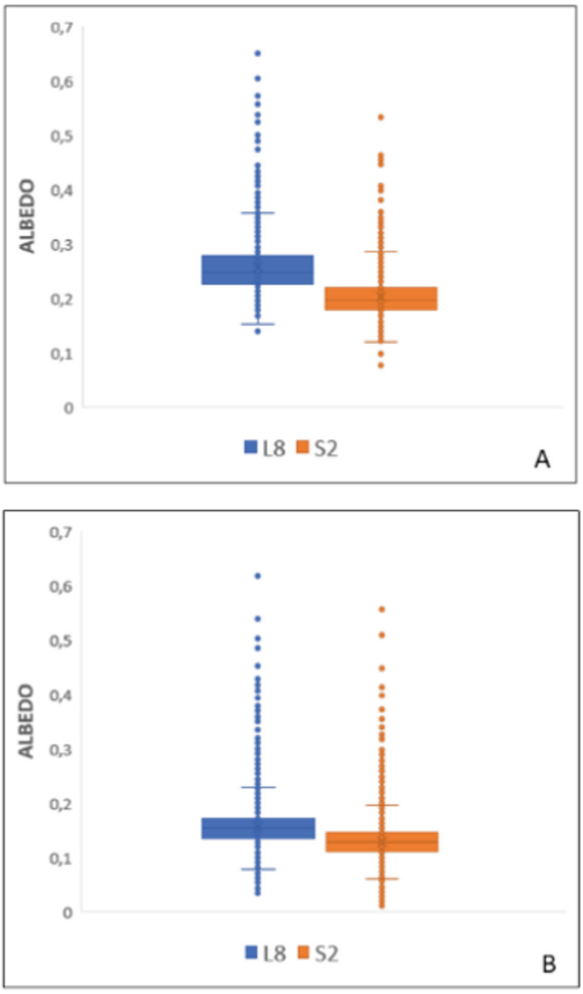

Fig. 7. Boxplots of albedo values in Bari (A) and Berlin (B), respectively. L8: Landsat 8; S2: Sentinel-2.

Conversely, "port areas" show a difference of about 0.04. This outcome is mainly due to the scattering problems of the sea and the different geometric resolution. Also, the classes "construction sites" and "forests" show a higher difference, about 0.05 and 0.04, respectively. Perhaps, this is due to the scarce presence of such LU/LC categories in Bari.

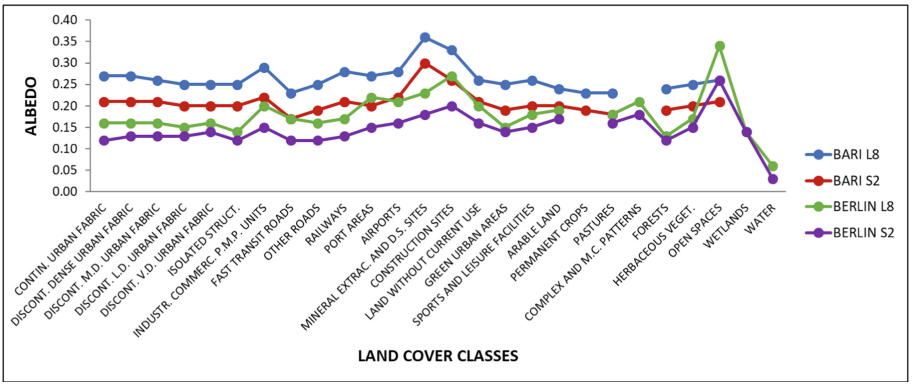

Fig. 8. Mean albedo value for each LU/LC class taken from Copernicus UrbanAtlas 2018. M.D.: medium density; L.D.: low density; V.D.: very low density; P.M.P.: public, military and private; D.S.: dump sites; M.C.: mixed cultivations. L8: Landsat 8; S2: Sentinel-2.

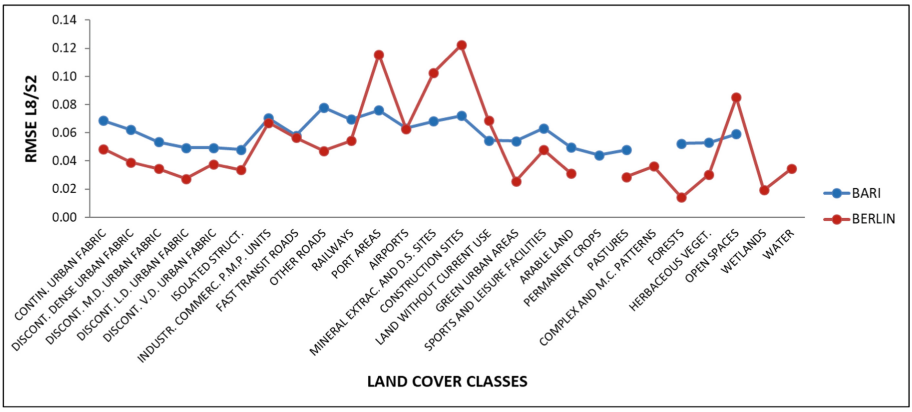

Fig. 9. RMSE values between L8 and S2 albedo estimations for each LU/LC class. M.D.: medium density; L.D.: low density; V.D.: very low density; P.M.P.: public, military and private; D.S.: dump sites; M.C.: mixed cultivations. L8: Landsat 8; S2: Sentinel-2.

4 Conclusion

The objective of this paper is to estimate land surface albedo using two different satellite datasets and to explore their potentialities over two study areas, the cities of Bari and Berlin, respectively. Such sites were selected because of their great diversity in terms of climatic and geo-morphological features. This gives the possibility to test algorithms performances in a diverse urban context. Indeed, this research contributes also to investigating LU/LC impact on albedo changes. Because of natural areas replacement with impervious material, the urbanization process influences urban climate, as well as land surface energy balance [5, 26, 38–41]. Therefore, investigating the albedo trend in urban areas may improve the knowledge of UHI phenomenon and identify the optimal strategy to face it [6, 9]. To achieve such a goal, two algorithms, the Silva *et al.* (2016) [20],

specific for Landsat 8 data, and the Bonafoni *et al.* (2020) [23] for Sentinel-2 images, were implemented. Their outcomes were satisfying results in terms of correlation, SD and RMSE albeit Landsat 8 algorithm provided higher mean values, for both study sites, than Sentinel-2 algorithm.

To implement the processing procedure, a proper JavaScript code was developed in GEE environment. It was preferred to desktop software because of its many advantages in comparison to desktop software, such as the capability to i) customize codes to meet users needs, ii) implement complex algorithms, and, lastly, iii) minimize acquisition and operational times [42]. At the same time, it also has some disadvantages such as the need to export maps, which have to be imported into another software like QGIS in order to improve the visualization of the results. Nevertheless, GEE can be recognized as the optimal tool for investigating satellite geospatial big data because of the benefits above mentioned.

Lastly, this paper introduces additional innovative elements in comparison to previous studies. Indeed:

1. potentialities of Landsat 8 and Sentinel-2 data were explored and compared;
2. algorithms performance was assessed by comparing their results both visually and statistically considering the whole case study and each LU/LC class.

References

1. Liu, Q., Wen, J., Qu, Y., He, T., Zhang, X., Wang, L.: Broadband albedo. In: Liang, S., Li, X., Wang, J. (eds.) Advanced Remote Sensing: Terrestrial Information Extraction and Applications, 1st edn, pp. 173–231. Academic Press, Cambridge (2012)
2. Capolupo, A., Monterisi, C., Barletta, C., Tarantino, E.: Google earth engine for land surface albedo estimation: comparison among different algorithms. In: Proceedings of SPIE 11856, Remote Sensing for Agriculture, Ecosystems, and Hydrology XXIII, p. 118560F. International Society for Optics and Photonics (2021)
3. Essential Climate Variables. https://gcos.wmo.int/en/essential-climate-variables. Accessed 28 Nov 2021
4. Voogt, J.A., Oke, T.R.: Thermal remote sensing of urban climates. Remote Sens. Environ. **86**(3), 370–384 (2003)
5. The Urban Heat Island (UHI) Effect. https://www.urbanheatislands.com/. Accessed 13 Dec 2021
6. Sangiorgio, V., Capolupo, A., Tarantino, E., Fiorito, F., Santamouris, M.: Evaluation of absolute maximum urban heat island intensity based on a simplified remote sensing approach. Environ. Eng. Sci. **39**(3), 296–307 (2022)
7. Capolupo, A., Monterisi, C., Saponaro, M., Tarantino, E.: Multi-temporal analysis of land cover changes using Landsat data through google earth engine platform. In: Proceedings of SPIE 11524, Eighth International Conference on Remote Sensing and Geoinformation of the Environment (RSCy2020), pp. 1152419. International Society for Optics and Photonics (2020)
8. Capolupo, A., Boccia, L.: Innovative method for linking anthropisation process to vulnerability. World Rev. Sci. Technol. Sustain. Dev. **17**(1), 4–22 (2021)

9. Trlica, A., Hutyra, L.R., Schaaf, C.L., Erb, A., Wang, J.A.: Albedo, land cover, and daytime surface temperature variation across an urbanized landscape. Earth's Future **5**, 1084–1101 (2017)
10. Lama, G.F.C., Sadeghifar, T., Azad, M.T., Sihag, P., Kisi, O.: On the indirect estimation of wind wave heights over the Southern Coast of Caspian sea: a comparative analysis. Water **14**(6), 843 (2022)
11. Lama, G.F.C., Crimaldi, M.: Remote sensing of ecohydrological, ecohydraulic, and ecohydrodynamic phenomena in vegetated waterways: the role of leaf area index (LAI). Biol. Life Sci. Forum **3**(1), 54 (2021)
12. Sadeghifar, T., Lama, G.F.C., Sihag, P., Bayram, A., Kisi, O.: Wave height predictions in complex sea flows through soft-computing models: case study of Persian Gulf. Ocean Eng. **245**, 110467 (2022)
13. Esposito, M., Crimaldi, M., Cirillo, V., Sarghini, F., Maggio, A.: Drone and sensor technology for sustainable weed management: a review. Chem. Biol. Technol. Agric. **8**(1), 1–11 (2021). https://doi.org/10.1186/s40538-021-00217-8
14. Capolupo, A., Monterisi, C., Sonnessa, A., Caporusso, G., Tarantino, E.: Modeling land cover impact on albedo changes in google earth engine environment. In: Gervasi, O., et al. (eds.) ICCSA 2021. LNCS, vol. 12955, pp. 89–101. Springer, Cham (2021). https://doi.org/10.1007/978-3-030-87007-2_7
15. Liang, S.: Narrowband to broadband conversions of land surface albedo I algorithms. Remote Sens. Environ. **76**, 210–238 (2000)
16. Tarantino, E.: Monitoring spatial and temporal distribution of sea surface temperature with TIR sensor data. Italian J. Remote Sens. **44**(1), 97–107 (2012)
17. Caprioli, M., Tarantino, E.: Identification of land cover alterations in the Alta Murgia National Park (Italy) with VHR satellite imagery. Int. J. Sustain. Dev. Plan. **1**(3), 261–270 (2006)
18. Capolupo, A., Saponaro, M., Fratino, U., Tarantino, E.: Detection of spatio-temporal changes of vegetation in coastal areas subjected to soil erosion issue. Aquat. Ecosyst. Health Manag. **23**(4), 491–499 (2020)
19. Sarzana, T., Maltese, A., Capolupo, A., Tarantino, E.: Post-processing of pixel and object-based land cover classifications of very high spatial resolution images. In: Gervasi, O., et al. (eds.) ICCSA 2020. LNCS, vol. 12252, pp. 797–812. Springer, Cham (2020). https://doi.org/10.1007/978-3-030-58811-3_57
20. da Silva, B.B., Braga, A.C., Braga, C.C., de Oliveira, L.M.M., Montenegro, S.M.G.L., Barbosa, J.B.: Procedures for calculation of the Albedo with OLI-Landsat 8 images: application to the Brazilian semi-arid. Revista Brasileira de Engenharia Agrícola e Ambiental **20**, 3–8 (2016)
21. Varghese, D., Radulović, M., Stojković, S., Crnojević, V.: Reviewing the potential of Sentinel-2 in assessing the drought. Remote Sens. **13**(17), 3355 (2021)
22. Vanino, S., et al.: Capability of Sentinel-2 data for estimating maximum evapotranspiration and irrigation requirements for tomato crop in Central Italy. Remote Sens. Environ. **215**, 452–470 (2018)
23. Bonafoni, S., Sekertekin, A.: Albedo retrieval from Sentinel-2 by new narrow-to-broadband conversion coefficient. IEEE Geosci. Remote Sens. Lett. **17**(9), 1618–1622 (2020)
24. Hird, J.N., DeLancey, E.R., McDermid, G.J., Kariyeva, J.: Google earth engine, open-access satellite data, and machine learning in support of large-area probabilistic wetland mapping. Remote Sensing **9**(12), 1315 (2017)
25. Gorelick, N., Hancher, M., Dixon, M., Ilyushchenko, S., Thau, D., Moore, R.: Google earth engine: planetary-scale geospatial analysis for everyone. Remote Sens. Environ. **202**, 18–27 (2017)
26. Martinelli, A., Kolokotsa, D.-D., Fiorito, F.: Urban heat island in Mediterranean coastal cities: the case of Bari (Italy). Climate **8**(6), 79 (2020)

27. Leone, A., Gobattoni, F., Pelorosso, R., Calace, F.: Nature-based climate adaptation for compact cities: green courtyards as urban cool islands. Plurimondi **18**, 83–110 (2020)
28. Peschechera, G., Tarantino, E., Fratino, U.: Crop water requirements estimation at irrigation district scale from remote sensing: a comparison between MODIS ET product and the analytical approach. In: Proceedings of SPIE 10773, Sixth International Conference on Remote Sensing and Geoinformation of the Environment (RSCy2018), p. 1077318. International Society for Optics and Photonics (2018)
29. Tarantino, E., Novelli, A., Aquilino, M., Figorito, B., Fratino, U.: Comparing the MLC and JavaNNS approaches in classifying multi-temporal LANDSAT satellite imagery over an ephemeral river area. Int. J. Agric. Environ. Inf. Syst. (IJAEIS) **6**(4), 83–102 (2015)
30. Vulova, S., Meier, F., Fenner, D., Nouri, H., Kleinschmit, B.: Summer nights in Berlin, Germany: modeling air temperature spatially with remote sensing, crowdsourced weather data, and machine learning. IEEE J. Sel. Top. Appl. Earth Observ. Remote Sens. **13**, 5074–5087 (2020)
31. Dugord, P.-A., Lauf, S., Schuster, C., Kleinschmit, B.: Land use patterns, temperature distribution, and potential heat stress risk – the case study Berlin, Germany. Comput. Environ. Urban Syst. **48**, 86–98 (2014)
32. Kühn, M., Gailing, L.: From green belts to regional parks: history and challenges of suburban landscape planning in Berlin. In: Amati, M. (ed.) Urban Green Belts in the Twenty-first Century, Chapter 10, pp. 185–202. Ashgate (2008)
33. Li, H., et al.: A new method to quantify surface urban heat island intensity. Sci. Tot. Environ. **624**, 262–272 (2018)
34. Urban Atlas 2018. https://land.copernicus.eu/local/urban-atlas/urban-atlas-2018. Accessed 26 Feb 2022
35. Allen, R.G., Tasumi, M., Trezza, R.: Satellite-based energy balance for mapping evapotranspiration with internalized calibration (METRIC) – model. J. Irrig. Drain. Eng. **133**(4), 380–394 (2007)
36. Taha, H.: Urban climates and heat islands: albedo, evapotranspiration, and anthropogenic heat. Energy Build. **25**, 99–103 (1997)
37. Waters, R., Allen, R., Tasumi, M., Trezza, R., Bastiaanssen, W.: SEBAL (surface energy balance algorithms for land). Idaho implementation. In: Advanced Training and Users Manual. Version 1.0 (2002)
38. Lai, S., Leone, F., Zoppi, C.: Spatial distribution of surface temperature and land cover: a study concerning Sardinia, Italy. In: Gervasi, O., et al. (eds.) ICCSA 2020. LNCS, vol. 12253, pp. 405–420. Springer, Cham (2020). https://doi.org/10.1007/978-3-030-58814-4_29
39. Crocetto, N., Tarantino, E.: A class-oriented strategy for features extraction from multidate ASTER imagery. Remote Sens. **1**(4), 1171–1189 (2009)
40. Novelli, A., Tarantino, E., Caradonna, G., Apollonio, C., Balacco, G., Piccinni, F.: Improving the ANN classification accuracy of Landsat data through spectral indices and linear transformations (PCA and TCT) aimed at LU/LC monitoring of a River Basin. In: Gervasi, O., et al. (eds.) ICCSA 2016. LNCS, vol. 9787, pp. 420–432. Springer, Cham (2016). https://doi.org/10.1007/978-3-319-42108-7_32
41. Boccia, L., Capolupo, A., Rigillo, M., Russo, V.: Terrace abandonment hazards in a Mediterranean cultural landscape. J. Hazardous Toxic Radioactive Waste 24(1) (2020)
42. Capolupo, A., Monterisi, C., Caporusso, G., Tarantino, E.: Extracting land cover data using GEE: a review of the classification indices. In: Gervasi, O., et al. (eds.) ICCSA 2020. LNCS, vol. 12252, pp. 782–796. Springer, Cham (2020). https://doi.org/10.1007/978-3-030-58811-3_56